Lisa M. Galle, George E. Cutsail III, Volker Nischwitz, Serena DeBeer and Ingrid Span*

# Spectroscopic characterization of the Co-substituted C-terminal domain of rubredoxin-2

https://doi.org/10.1515/hsz-2018-0142
Received January 31, 2018; accepted April 25, 2018

**Abstract:** *Pseudomonas putida* rubredoxin-2 (Rxn2) is an essential member of the alkane hydroxylation pathway and transfers electrons from a reductase to the membrane-bound hydroxylase. The regioselective hydroxylation of linear alkanes is a challenging chemical transformation of great interest for the chemical industry. Herein, we report the preparation and spectroscopic characterization of cobalt-substituted *P. putida* Rxn2 and a truncated version of the protein consisting of the C-terminal domain of the protein. Our spectroscopic data on the Co-substituted C-terminal domain supports a high-spin Co(II) with a distorted tetrahedral coordination environment. Investigation of the two-domain protein Rxn2 provides insights into the metal-binding properties of the N-terminal domain, the role of which is not well understood so far. Circular dichroism, electron paramagnetic resonance and X-ray absorption spectroscopies support an alternative Co-binding site within the N-terminal domain, which appears to not be relevant in nature. We have shown that chemical reconstitution in the presence of Co leads to incorporation of Co(II) into the active site of the C-terminal domain, but not the N-terminal domain of Rxn2 indicating distinct roles for the two rubredoxin domains.

**Keywords:** AlkG; iron-sulfur protein; metal substitution; *Pseudomonas putida* GPo1; rubredoxin.

***Corresponding author: Ingrid Span,** Institut für Physikalische Biologie, Heinrich-Heine-Universität Düsseldorf, Universitätsstr. 1, D-40225 Düsseldorf, Germany, e-mail: ingrid.span@uni-duesseldorf.de. http://orcid.org/0000-0002-2892-4825
**Lisa M. Galle:** Institut für Physikalische Biologie, Heinrich-Heine-Universität Düsseldorf, Universitätsstr. 1, D-40225 Düsseldorf, Germany
**George E. Cutsail III and Serena DeBeer:** Max Planck Institute for Chemical Energy Conversion, D-45470 Mülheim an der Ruhr, Germany
**Volker Nischwitz:** Central Institute for Engineering, Electronics and Analytics (ZEA-3), Forschungszentrum Jülich, D-52425 Jülich, Germany

## Introduction

The regioselective introduction of molecular oxygen onto the unreactive terminal methyl group of alkanes is a relevant and challenging chemical transformation. Saturated hydrocarbons are among the most abundant naturally occuring organic molecules and it would be desirable to be able to transform them into higher-value compounds, such as chemicals or synthetic fuels (Bordeaux et al., 2012). Linear alkanes are also among the most difficult to oxyfunctionalize at the terminal position in a controllable manner at lower temperature. However, as linear alcohols or acids are extremely desirable potential feedstocks for the chemical industry, there is an urgent need for novel catalysts for selectively oxidizing the terminal methyl groups (Thomas et al., 2001). The bacterium *P. putida* (formerly known as *P. oleovorans*) can realize this reaction with the alkane monooxygenase AlkB, an integral membrane-bound diiron protein, in conjunction with its redox partner Rxn2, also referred to as AlkG, and the NADH-dependent reductase AlkT (Kok et al., 1989). Rxn2 is one of two rubredoxins in the *alkBAC* operon and transfers electrons from the cytoplasmic reductase to the active center of the membrane-bound alkane hydroxylase.

Rubredoxins are the smallest and simplest type of iron-sulfur proteins, and they serve as electron carriers in the cell (Lovenberg and Sobel, 1965). They usually contain one mononuclear iron-binding site, with the iron coordinated by the thiol groups of four cysteine residues in a tetrahedral symmetry (Figure 1), as seen in the crystal structure of *Clostridium pasteurianum* rubredoxin (Maher et al., 2004). *Pseudomonas putida* Rxn2 is unique in that it consists of two rubredoxin-like domains, an N-terminal and a C-terminal metal-binding domain connected by a 70-amino-acid linker (Lode and Coon, 1971). The presence of two domains results in an unusually high molecular weight of 19 kDa compared to other rubredoxins with a molecular mass of approximately 6 kDa. The molecular structure of Rxn2 was determined by nuclear magnetic resonance (NMR) spectroscopy and X-ray scattering and reveals that both domains adopt a similar globular fold, separated by the linker region that keeps the two domains separated in solution (Perry et al., 2004). It was speculated if the *alkG* gene is the product of a gene duplication event

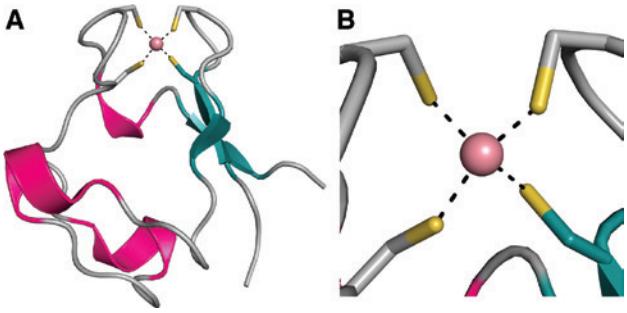


**Figure 1:** Structure of Co-substituted rubredoxin from *Clostridium pasteurianum* (Maher et al., 2004).
(A) Overall architecture of the protein and (B) close-up of the Co-binding site. The protein is shown as cartoon model in gray with the secondary structure elements colored in pink (α-helix) and teal (β-sheet). The side chains of the four cysteines that involved in metal coordination are depicted as sticks with the sulfur atoms colored in yellow and the Co ion is shown as sphere colored in light pink.

(Lee et al., 1997). However, sequencing and functional analysis have provided evidence that the N-terminal and the C-terminal domain belong to two types of rubredoxins, AlkG1 and AlkG2, respectively (van Beilen et al., 2002). The degree of conservation amongst AlkG1-type domains and the significant differences to AlkG2-type domains in conjunction with mutational studies suggest that *alkG* is not just the product of gene duplication, but plays a role in alkane hydroxylation that has not been fully understood yet (van Beilen et al., 2002).

Rubredoxins are also frequently used as model systems for iron-sulfur proteins as their small size, solubility and robustness facilitate protein production. In particular, they were successfully utilized to study the replacement of the native metal in iron-sulfur proteins by transition metals other than iron. Successful attempts have been made to substitute the native metal in these proteins by metals, such as Co, Ni, Zn, Ga, Cd, and Hg (May and Kuo, 1978; Moura et al., 1991; Dauter et al., 1996; Lee et al., 1997; Maher et al., 2004). Co is a particularly useful probe and label of proteins, as it exhibits characteristic spectra (Maret and Vallee, 1993). The preparation the Co(II)-substituted *P. putida* Rxn2 has previously been reported (May and Kuo, 1978) as the first example of metal substitution by chemical reconstitution in an iron-sulfur protein and their results indicate that there is no evidence for nonequivalence of the two metal-binding sites.

The N-terminal domain including a portion of the linker region was reported to be colorless after purification (Perry et al., 2001) and the native form of *P. putida* Rxn2 is isolated bound to one iron (Lee et al., 1997), indicating that the two domains may not be equivalent. This hypothesis is also supported by NMR studies of the Cd-substituted form of Rxn2 that show two distinct Cd resonances, which indicates different chemical environments of both nuclei. Despite several studies and a high-resolution structure, the role of the two metal-binding domains of Rxn2 remains unclear. A detailed understanding of the recognition of the physiological redox partners as well as the electron transfer mechanism of this redox system would be of great interest for potential biotechnological applications (Tsai et al., 2017). Herein, we report the incorporation of Co into the active site of the C-terminal domain of rubredoxin-2 and full-length Rxn2 from *P. putida* GPo1 and a detailed spectroscopic study of the properties of the native and truncated version of the protein.

# Results

## Incorporation of Co into the C-terminal domain of Rxn2

The N-terminal domain of *P. putida* Rxn2 is less stable compared to the C-terminal domain, thus, we have generated a construct encoding for the amino acids 51-173 (Perry et al., 2001). We have expressed the truncated and the full-length version of the *alkG* gene and isolated the resulting gene products. The proteins revealed a reddish color, indicating the presence of a (partially) iron-bound form. To remove the native metal from the active site, the protein samples were denatured in the presence of 10% trichloroacetic acid (TCA). Refolding the proteins in 4-(2-hydroxyethyl)piperazine-1-ethanesulfonic acid (HEPES) buffer in the presence of 10-fold excess tris(2-carboxyethyl)phosphine (TCEP) and equimolar cobalt chloride ($CoCl_2$) under anerobic conditions, yields the Co-derivatives of Rxn2-CT as well as Rxn2.

The success of the reconstitution reaction was assessed by electronic absorption spectroscopy (EAS), as the electronic spectrum of a Co site is very sensitive to the geometry of its coordination environment. The electronic absorption spectrum of the C-terminal domain of Rxn2 (Figure 2A) reveals absorption maxima in the near ultraviolet (UV) and visible (Vis) region. The band at 350 nm originates from Cys-$S^-$ to Co(II) transitions with a molar absorptivity of 2232 $M^{-1}$ $cm^{-1}$ (Table S1) (Curdel and Iwatsubo, 1968; Drum and Vallee, 1970; McMillin et al., 1974). Four bands with lower intensity in the visible range of the spectrum at 623 nm, 662 nm, 690 nm, and 753 nm originate from d-d ligand field (LF) transitions and are in agreement

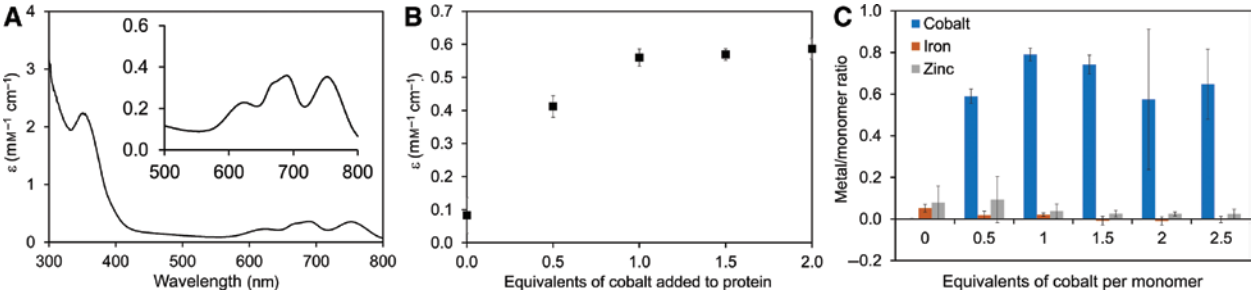


**Figure 2:** Co-binding to the C-terminal domain of Rxn2.
(A) Electronic absorption spectrum of Rxn2-CT, plotted as molar absorptivity (ε) vs. wavelength. The inset shows a close-up view of the ligand field transitions (500–800 nm). (B) Titration of $Co^{2+}$ to apo protein presented as molar absorptivity (ε) at 750 nm vs. the equivalents of Co added to the apo protein and are the average ± one standard deviation of three independent trials. (C) The metal content is expressed per monomer with data from three independent measurements averaged ± one standard deviation. Values for Co are shown in blue, iron in orange, and zinc in gray. The apo protein for both experiments was prepared by TCA-precipitation, followed by reconstitution of the protein in absence of Co.

with a distorted tetrahedral symmetry of a high-spin Co(II) complex (Sugiura, 1978).

## Binding of Co to the truncated version of Rxn2

As a next step, we wanted to investigate, if the metal ion can be incorporated into the apo protein after the reconstitution or whether the metal ion is required for proper refolding of the precipitated sample. Subsequent to TCA precipitation of the isolated protein, we reconstituted the protein in the presence and absence of $CoCl_2$. Circular dichroism (CD) spectra suggest that the C-terminal domain of Rxn2 is capable of adopting a similar structure in the apo form compared to the Co-bound form (Supplementary Figure S1). The CD spectra of apo and Co-bound Rxn2-CT are virtually identical, indicating that the secondary structure, and most likely the tertiary structure, is not particularly affected by the presence of the metal.

After establishing that metal-binding does not alter the structure of Rxn2-CT, we titrated various equivalents of $CoCl_2$ to the protein that was reconstituted in its apo form, and monitored the metal-binding by EAS (Figure 2B and Supplementary Figure S2). The bands deriving from the LF transitions are more sensitive to the incorporation of Co, thus, we monitored the increase of the band at 750 nm to determine the amounts of Co needed to fully occupy the active site. Our results suggest that an equimolar ratio of Co fully loads the metal-binding site. To avoid the binding of excess metal, we therefore carried out all following sample preparations using one equivalent of Co per metal-binding site.

To quantify the amount of metal that binds to Rxn2-CT, we titrated 1–5 equivalents $CoCl_2$ to the apo protein and determined the amount of Co, Fe, and Zn by inductively coupled plasma-mass spectrometry (ICP-MS). To reduce the background, we exchanged the buffer using Sephadex G-25 chromatography after incubating the protein with the Co solution in the presence of a reducing agent. Upon overnight incubation with an equimolar amount of Co, we found that ~0.8 mol equivalent of metal were retained (Figure 2C). Exposing the protein to a 2.5-fold excess of Co did not increase the amount of Co that was retained by the protein. The metal quantification shows that one Co is bound by Rxn2-CT and the slightly lower value could be explained by the inability of a part of the protein to bind Co, as a result of misfolding, or the inaccuracy of protein concentration determination by absorbance at 280 nm (Edelhoch, 1967). The extinction coefficient was calculated using the protein analysis tool ProtParam on the ExPASy server (Gasteiger et al., 2005). A comparison of various protein concentration determination methods, including infrared (IR) spectroscopy (Strug et al., 2014), the Bradford assay (Bradford, 1976) and absorbance at 280 nm confirms that the protein concentration obtained by absorbance is higher than with the other methods (Figure S3). An overestimation of the protein concentration leads to an underestimation of the metal per monomer ratio, which could explain the 0.8 mol equivalents of Co. We have also performed electrospray ionization-mass spectrometry (ESI-MS) to check for oxygenated species that could prevent the binding of Co to the thiol groups and our data show that no oxygenated cysteines are present in Rxn2-CT (Figure S4). Taken together, our ICP-MS results confirm our initial finding that an equimolar amount of

Co is sufficient to occupy the metal-binding site of the C-terminal domain of Rxn2.

## Characterization of the Co-binding site

To confirm the interpretation of the electronic absorption spectrum and to obtain more detailed insights into the coordination environment of the Co ion, we performed electron paramagnetic resonance (EPR) spectroscopy and high-energy resolution fluorescence detected (HERFD) X-ray absorption spectroscopy (XAS) (Castillo et al., 2017) including extended X-ray absorption fine structure (EXAFS) analysis. The continuous-wave X-band EPR spectrum of Rxn2-CT exhibits a typical high-spin Co(II) $S=3/2$ signal (Figure 3A), where the zero-field splitting is larger than the incident energy (~0.3 $cm^{-1}$ at X-band frequencies). The observed spectrum is of transitions within the $M_S = \pm 1/2$ manifold, and exhibits a $g_{\perp} \sim 3.9$, typical of tetrahedral symmetry (Makinen et al., 1985). The $S=3/2$ spectrum may be represented as a $S=1/2$ spin system, as previously demonstrated (Shimizu et al., 1983) and simulated by the effective, observed $g$-values. The spectrum is found to possess a slightly rhombic $g_{eff}$-tensor of [4.92, 3.71, 2.15], within the range of expected $g$-values for pseudo-tetrahedral symmetry (Bencini et al., 1981) and other pseudo-tetrahedral protein or other synthetic tetrathiolate Co(II) centers (Makinen et al., 1985; Good and Vasak, 1986; Fukui et al., 1991; Zielazinski et al., 2012). Unresolved hyperfine splitting of the $I=7/2$ $^{57}$Co nuclei is a significant contributor to the broad anisotropic EPR linewidths observed.

HERFD XAS of the Rxn2-CT exhibits a spectrum typical of Co(II) species in agreement with Co(II) species observed by EPR (Figure 3B). Particularly, the intense pre-edge feature of the HERFD XAS spectrum at ~7709.7 eV is indicative of the coordination geometry of the Co ions. As the pre-edge transition is formally a 1*s*–3*d* transition and dipole forbidden, it is inherently weak. Significant loss of centrosymmetry of a metallocenter results in mixing of the metal's 4*p* orbitals with the 3*d* orbitals. The dipole allowed 1*s*–4*p* transition character increases the pre-edge intensity, indicating reduced symmetry of the metal coordination environment (Westre et al., 1997). The intense pre-edge observed in Figure 3B is consistent with a pseudo-tetrahedral Co center (Gavel et al., 1998).

The Co EXAFS spectrum of the Rxn2-CT exhibits strong oscillations typical of sulfur backscattering atoms.

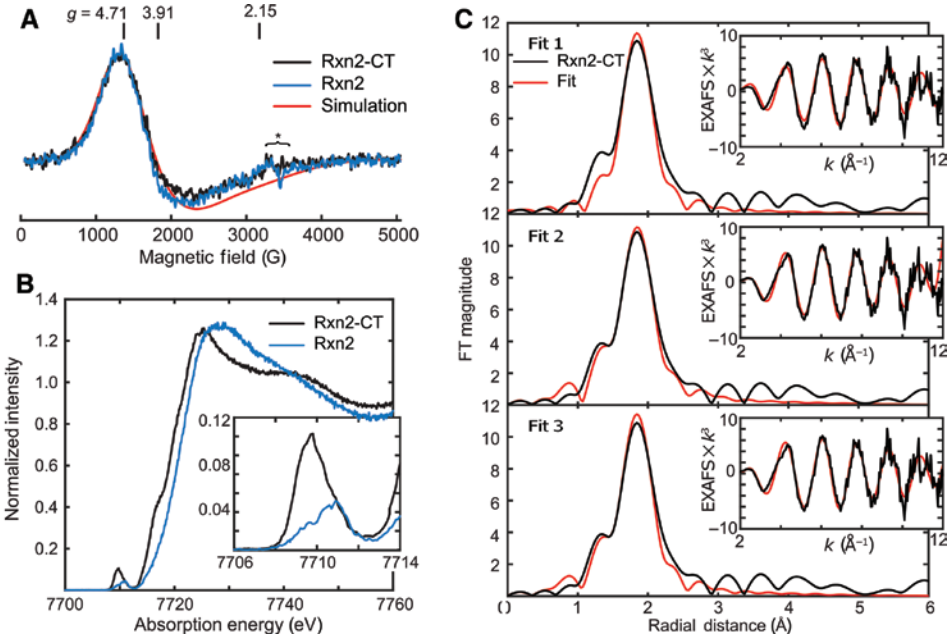


**Figure 3:** Spectroscopic characterization of the C-terminal domain of Rxn2 and the full-length protein.
(A) X-band (9.63 GHz) EPR spectra of Rxn2-CT (black) and Rxn2 (blue), collected at 4 K with 100 kHz field modulation and 6.0 G modulation amplitude employing an 82 ms time constant and a 167 s scan time. Simulated EPR spectrum of Rxn2-CT (red) has a $g_{eff}$ = [4.92, 3.71, 2.15] and large line broadenings of [1150, 4500, 4000] MHz. The asterisk marks a copper background signal attributed to the EPR cavity. (B) Intensity normalized Co K-edge HERFD XAS spectra of Rxn2-CT (black) and Rxn2 (blue) with the pre-edge features expanded within the figure inset. (C) Non-phase shifted Fourier Transform spectrum of the $k^3$-weighted EXAFS of Rxn2-CT (black) with each of the three described EXAFS fits (red). The raw $k^3$-weighted EXAFS and corresponding fits are in each figure panel's inset.

**Table 1:** EXAFS fit parameters for Rxn2-CT.

| Amp | n | Path | $R$ (Å) | ± | $\sigma^{2a}$ | ± |
|---|---|---|---|---|---|---|
| Fit 1 | | | | | | |
| | 4 | Co-S | 2.296 | 0.010 | 4.94 | 0.60 |
| $\Delta E_0 = 1.709$ eV | | | | $F$-value[b] = 27.8 | | |
| Fit 2 | | | | | | |
| | 3 | Co-S | 2.304 | 0.013 | 2.34 | 0.78 |
| | 1 | Co-O | 1.987 | 0.036 | 1.11 | 3.25 |
| $\Delta E_0 = 2.309$ eV | | | | $F$-value = 10.2 | | |
| Fit 3 | | | | | | |
| 90% | 4 | Co-S | 2.297 | 0.014 | 4.58 | 0.63 |
| 10% | 6 | Co-O | 1.953 | 0.057 | 3.00[c] | N/A |
| $\Delta E_0 = 1.159$ eV | | | | $F$-value = 12.6 | | |

[a]Debye-Waller like value with units of $1\times10^{-3}$ Å$^2$.

[b]$F = 1000\times\sum_{i=1}^{n}(\text{data}_i - \text{fit}_i)^2 / \sum_{i=1}^{n}\text{data}_i^2$.

[c]Value was fixed for this fit.

The $k^3$-weighted EXAFS spectrum (Figure 3C) appears to be formed from a single dominant beat pattern, arising from degenerate Co-S backscattering. The non-phase shifted Fourier transform of the EXAFS yields a prominent radial shell centered at $R = 1.9$ Å. The EXAFS is well modeled with four degenerate sulfur backscattering atoms at a mean distance of 2.30 Å, Figure 3C, Table 1, Fit 1. The fitted Debye-Waller like $\sigma^2$-value of the Co-S path is $4.94\times10^{-3}$ Å$^2$, a moderate amount of disorder as expected for the four-fold degenerate path. Attempts to split the degenerate Co-S scattering paths do not yield improved fits or physical fit parameters. The theoretical resolution of the FT spectrum is approximately $\Delta R = 0.17$ Å, not allowing for differences in the Co-S paths smaller than this to be separated.

As the FT spectrum is well fitted by the n = 4, Co-S scattering interaction alone, however, a shorter scattering distance is not fully fit at the shoulder at $R$ ~1.4 Å in the FT EXAFS spectrum. This feature correlates to a Co backscattering distance of ~2.0 Å and is too short for a Co-thiolate bond. Therefore, a light Z-atom coordination (i.e. N or O) is more likely. Fitting of the EXAFS with a $CoS_3[O/N]_1$ coordination environment significantly improves the fit as observed by the decrease in the $F$-value of Fit 2 compared to Fit 1 (Table 1). However, it must also be considered that this scattering could arise from the possibility of second minority Co species such as a hexaaquacobalt ion in the presence of the $CoS(Cys)_4$ site. Including a six-fold degenerate Co-O scattering paths from $Co(H_2O)_6$ with a fixed $\sigma^2$-value of $3.0\times10^{-3}$ Å$^2$ for the well-ordered interaction, a mean Co-O distance of 1.95 Å is fit at only 10% of the relative EXAFS amplitude to the n = 4 Co-S scattering path (Fit 3, Figure 3C and Table 1). This corresponds to a 9:1 ratio of $CoS_4$:$Co(H_2O)_6$. The $F$-value of this fit rivals that of Fit 2 of an $CoS_3[O/N]_1$ coordination sphere, not allowing for immediate discrimination between these two possibilities. A small ~10% Co impurity is not expected to be resolved from the broad pseudo-tetrahedral Co EPR spectrum.

## Differential occupancy of the metal sites in Rxn2

To obtain more insights into the metal-binding properties of the N-terminal domain of Rxn2, we investigated the full-length protein and compared the results to the C-terminal domain of the protein. As the N-terminal domain of Rxn2 is less stable, we have chosen this indirect approach to obtain more information on the role of

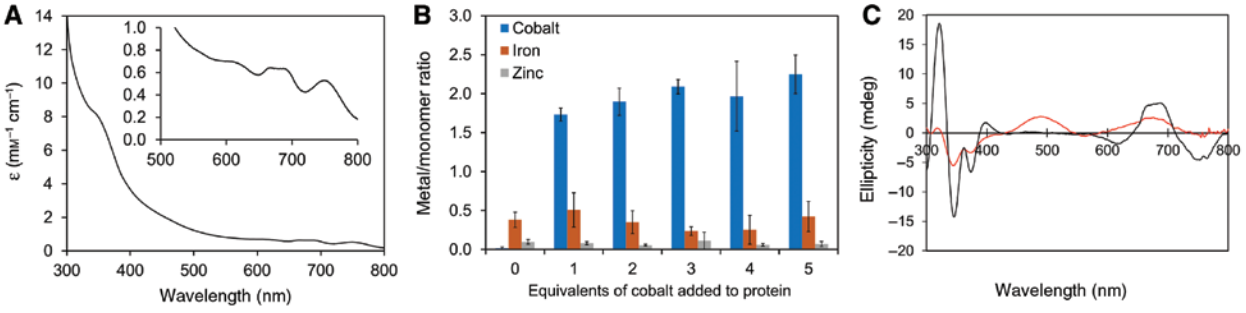


**Figure 4:** Binding of Co to full-length Rxn2.
(A) Electronic absorption spectrum, plotted as molar absorptivity (ε) vs. wavelength. The inset shows a close-up view of the ligand field transitions (500–800 nm). (B) The metal content per monomer is plotted vs. the equivalents of Co added to each protein monomer, with Co in blue, iron in orange, and zinc in gray. Data from three independent measurements were averaged ± one standard deviation. (C) Circular dichroism spectra in the near-UV and visible range of Rxn2-CT (black) and full-length Rxn2 (red). The isolated protein was precipitated using TCA and reconstituted in the presence of Co and TCEP. The final protein concentration of both samples was 0.5 mM.

the second rubredoxin domain. The electronic absorption spectrum of Co-substituted Rxn2 normalized per mole of protein (Figure 4A) displays similar maxima at 350 nm as well as in the 600–800 nm region compared to the C-terminal domain of Rxn2. Both samples for EAS, Rxn2-CT and Rxn2, were prepared according to the same protocol. Briefly, the isolated protein was precipitated by TCA, followed by reconstitution in the presence of 10-fold excess TCEP and equimolar amounts of $CoCl_2$ under anaerobic conditions. Excess reactants and impurities were removed by Sephadex G-25 chromatography. The molar absorptivity at a wavelength of 750 nm is 0.53 $mM^{-1}$ $cm^{-1}$ for Rxn2 and 0.35 $mM^{-1}$ $cm^{-1}$ for Rxn2-CT, suggesting that more than one Co binds to the full-length protein.

To determine the metal content of Rxn2, we prepared apo Rxn2 and treated the protein with 1–5 eq. of Co per monomer. After removing excess metal ions from the solution the amount of Co, Fe and Zn that was retained by the protein was determined using ICP-MS (Figure 4B). The results indicate that ~2 equivalents of Co bind to each Rxn2 monomer, which is consistent with the presence of two metal-binding domains.

The results of the metal content analysis are also consistent with the values of the molar absorptivity of the LF transition at 750 nm. One major obstacle for comparing the electronic absorption spectra of the C-terminal domain to the full-length protein is the high background of the Rxn2 spectrum. To overcome this limitation, we have recorded circular dichroism spectra in the near-UV and visible range. The bands deriving from ligand-to-metal charge transfer (LMCT) and LF transitions split up into maxima and minima in the CD spectra of Rxn2 and Rxn2-CT (Figure 4C), allowing a clearer view on spectral changes. To facilitate comparability, both samples were adjusted to a final protein concentration of 0.5 mM. Considering that full-length Rxn2 consists of two domains with one metal-binding site each, the overlay of the Rxn2 and Rxn2-CT proteins strongly indicates that only one site of Rxn2 is occupied by Co(II). The presence of the same bands for the Rxn2 sample compared to the Rxn2-CT indicate that the C-terminal domain of Rxn2 binds Co(II) in its active site, whereas, the metal-binding site of the N-terminal domain remains free.

Surprisingly, CD spectroscopy revealed another transition at 490 nm for the full-length Rxn2 protein that is not resolved within the EAS. This transition is likely attributable to a low-spin Co(III) species, as supported by the approximate +1 eV shift of the Co HERFD XAS edge energy (Figure 3B). The observed X-ray absorption spectrum of full-length Rxn2 is a convolution of the Co(II) site of the C-terminal and the Co(III) of the N-terminal domain. The EXAFS of full-length Rxn2, albeit poorer quality, indicates coordination of lighter atoms at shorter bond lengths (Figure S5). While there is a two-fold increase in the amount of Co in Rxn2 compared to Rxn2-CT, EPR spectroscopy of Rxn2 and Rxn2-CT at equal protein concentrations, exhibits equivalent Co(II) spectral intensities (Figure 3A). Therefore, the additional Co within the full-length Rxn2 protein is an EPR-silent Co(III) ion, an oxidation-state supported by the HERFD XAS spectrum (Figure 3B). The presence of an alternative Co-binding site in the N-terminal domain explains the observation that two Co ions bind per Rxn2 monomer (Figure 4B).

To compare the structural changes of Rxn2-CT and Rxn2, we have collected far-UV CD spectra of both proteins as isolated, in the apo and in the Co-substituted form

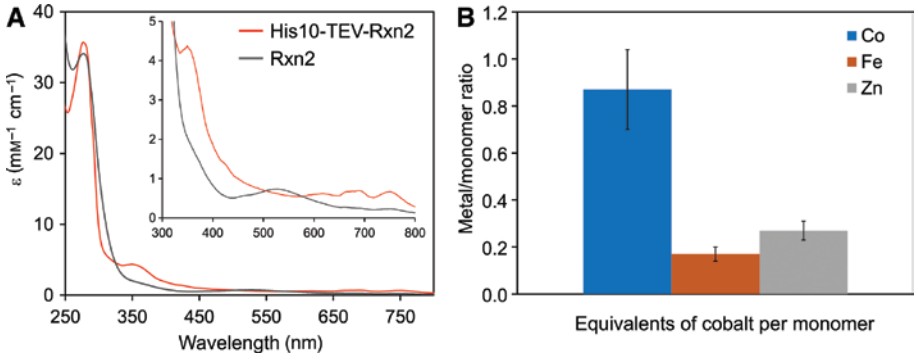


**Figure 5:** Metal content of Rxn2 isolated from M9 minimal medium containing $CoCl_2$.
(A) Electronic absorption spectrum, plotted as molar absorptivity ($\varepsilon$) vs. wavelength with the protein after the first affinity chromatography step shown in red and the protein after the TEV cleavage shown in gray. The inset shows a close-up view of the LMCT and ligand field transitions (300–800 nm). (B) The metal content of the isolated protein was determined by ICP-MS and is expressed per monomer protein with data from three independent measurements averaged ± one standard deviation. Values for Co are shown in blue, iron in orange, and zinc in gray.

(Figure S1). As previously stated, the C-terminal domain of Rxn2 does not undergo significant structural rearrangements upon removal of the native metal or incorporation of Co into the active site. However, we see a change in the spectrum from the isolated, Fe-bound form of Rxn2 and the apo protein, suggesting the loss of secondary structure over the denaturation and refolding process. The deviation of the CD spectrum of the Co-substituted Rxn2 could be explained by a lower protein concentration of the sample due to the inaccuracy of the protein concentration determination method. The loss of the secondary structure upon Co-binding is in conflict with the observation for the C-terminal domain and seems unlikely.

To elucidate the biological relevance of the second Co(III) binding site in the full-length protein, we adapted cells to an Fe-depleted and Co-supplemented medium, followed by cultivation of the cells in large scale and isolation of the Rxn2 protein. The protein obtained according to this protocol (Majtan et al., 2011) was purified by Co TALON affinity chromatography, then analyzed by EAS as well as ICP-MS (Figure 5). Subsequently, the affinity tag was removed by tobacco edge virus (TEV) cleavage in presence of 1,4-dithiothreitol (DTT) and ethylenediaminetetraacetic acid (EDTA), the protein was then separated from the uncleaved protein as well as the protease by another affinity chromatography step and analyzed by EAS. The His10-TEV-Rxn2 protein reveals spectral features identical to the reconstituted Rxn2-CT and 0.9 mol Co per monomer, indicating that only one of the metal-binding domains is occupied by Co. After treatment with DTT and EDTA during the TEV digestion reaction, the spectral features characteristic for the tetrathiolate coordination disappear and another peak at 530 nm appears that could derive from a Co(III) species. The ICP-MS results show that the protein isolated from Fe-depleted minimal media still contains Fe impurities, which might compete with Co for the active site of Rxn2. Notably, a significant amount of Zn also binds to the protein and possibly binds to the active site of the N-terminal domain.

## Discussion

We have established that the C-terminal domain of *P. putida* Rxn2 is an excellent model system for the replacement of the native metal of an iron-sulfur protein by Co. A previous study has reported the higher stability of the C-terminal domain compared to the N-terminal domain (Perry et al., 2001). Thus, we assumed that Rxn2-CT would be a suitable model system to study the incorporation of Co into the metal-binding site of an iron-sulfur protein.

The data reported here show that Co binds to the active site of apo Rxn2-CT (Figure 2A). Titration experiments suggest that one equivalent of $CoCl_2$ is sufficient to occupy the metal-binding site of the protein (Figure 2B). Addition of equimolar amount of Co leads to a metal content of ~0.8 equivalents of Co per monomer (Figure 2C). Tyrosine, tryptophan, and cysteine absorbance at 280 nm (Edelhoch, 1967; Gill and von Hippel, 1989) was used to determine the protein concentration of all samples. The extinction coefficient was determined based on the protein sequence and may vary with the amino acid composition. Thus, we compared the protein concentration method with IR spectroscopy (Strug et al., 2014) and with the Bradford assay (Bradford, 1976) that is based on absorbance of a dye in relation to a standard protein. Our results suggest that the protein concentration measured by absorbance at 280 nm is reliable for the full-length Rxn2 and overestimates the concentration of Rxn2-CT. This indicates that the metal content of Rxn2-CT is virtually one Co per monomer.

Metal analysis by ICP-MS (Figure 3B) and EXAFS (Figure 4C) of Rxn2-CT suggest that a large fraction of the protein (>90%) is reconstituted in the Co-bound form. In addition, the secondary and tertiary structure seem not be altered by the replacement of iron with Co, as observed by the far-UV spectra (Figure S1). Accordingly, the Co-substituted protein is well behaved, also at high protein concentrations, which is essential for preparing homogeneous and monodisperse samples for spectroscopic techniques.

The electronic absorption spectrum (Figure 2A) is consistent with previously reported spectra on Co-derivatives from other organisms or model complexes (Anglin and Davison, 1975; May and Kuo, 1978; Moura et al., 1991). The maxima at 350 nm can be assigned to a LMCT transition, whereas the bands in the 600–800 nm region originate from LF transition, which is indicative for a distorted tetrahedral high-spin Co(II) site. In comparison to the values of the molar absorptivity for the LF transitions found in literature that range of 335–645 $M^{-1}$ $cm^{-1}$ (Moura et al., 1991) and 1034–1232 $M^{-1}$ $cm^{-1}$ (May and Kuo, 1978), we observe maxima in the range of 229–359 $M^{-1}$ $cm^{-1}$ (Table S1). One possible explanation for this discrepancy could be differences in the background of the spectra, which is above 600 $M^{-1}$ $cm^{-1}$ (May and Kuo, 1978) compared to ~100 $M^{-1}$ $cm^{-1}$ in the spectrum presented in Figure 2A.

To obtain more detailed insights into the coordination environment of the protein-associated Co ion, we characterized the Co-substituted form of Rxn2-CT using EPR spectroscopy and HERFD XAS. The data presented here are in excellent agreement with a high-spin Co(II) center

of reduced symmetry (pseudo-tetrahedral). The deviation from the tetrahedral coordination environment is consistent with the $D_{2d}$ symmetry of the metal site observed in the crystal structure of metal-substituted derivatives of *C. pasteurianum* rubredoxin (Maher et al., 2004). The EXAFS analysis indicates majority thiolate ligation to the Co center, consistent with $Co(Cys)_4$ coordination environment. However, light-atom backscattering is observed, arising from either a 3S1(O/N) coordination sphere or a second minority Co species such as $[Co(H_2O)_6]$. Discriminating between these is challenging as a minority component, 10% or less as suggested by the EXAFS analysis, will not be immediately apparent in the HERFD XAS spectrum and the broad line widths of the EPR spectrum do not allow for multiple species to be resolved. However, the EXAFS fit with a 3S1(O/N) coordination environment results in very small disorder values ($\sigma^2$), smaller than anticipated for degenerate paths and also smaller than other pseudo-tetrahedral Co centers (Gavel et al., 1998; Zielazinski et al., 2012). Rejecting the 3S1(O/N) coordination scenario, the Co center can be reliably assigned as tetrathiolate coordinated and up to a 10% contamination of $[Co(H_2O)_6]$ or similar octahedrally coordinated species. This is in good agreement with the features observed in the absorption spectrum, discussed above.

Full-length Co-Rxn-2 has previously been characterized (May and Kuo, 1978; Lee et al., 1997; Perry et al., 2001), however, our data lead to new conclusions about the properties of the two rubredoxin-type domains. Metal-binding studies with Rxn2 (Figure 4A and B) indicate that Co binds to the active site and that two Co ions are retained by the full-length protein. The immediate conclusion would be that each Co ion is coordinated by four thiols in the active site of the N- and C-terminal domain, suggesting the equivalence of both rubredoxin domains, as has been proposed previously (May and Kuo, 1978). Metal analysis of Rxn2 also supports the binding of two metal ions per protein, indicating full occupancy of both metal-binding sites. Interestingly, the near-UV and visible CD spectra of the Co-reconstituted Rxn2-CT and Rxn2 reveal two Co species for the two domain protein. The broad band at 490 nm is not consistent with a cysteine-coordinated Co(II) species and is tentatively assigned to a low-spin Co(III) species. Another possibility would be that the 490 nm band derives from $Co(H_2O)_6$, however, as both proteins were prepared according to the same protocol, it is highly unlikely that only one sample would have a significant amount of free Co(II) ions. Taken together, the CD spectroscopy data indicate that only the active site of the C-terminal domain of Rxn2 is occupied by Co(II), whereas the N-terminal domain is not binding Co or only a very small fraction of the protein is capable of incorporating Co in the active site.

The Co content of Rxn2 reported in a previous study (May and Kuo, 1978) is similar to our ICP-MS results, we propose though that one of the Co ions is coordinated to an unspecific metal-binding site in the N-terminal region. Interestingly, May et al., observe a band at 470 nm in the electronic absorption spectrum of Co-Rxn2, which was tentatively assigned to a second charge-transfer transition. Assuming that both metal-binding sites in Rxn2 are equivalent, we also should see this band in the electronic absorption and CD spectra of Rxn2-CT, which is not the case (Figures 2A and 4C). In addition, this band was also not observed in Co-rubredoxin from *Desulfovibrio gigas* (Moura et al., 1991). We speculate that the 470 nm band derives from the interaction of Co in solution with the reducing agent, β-mercaptoethanol, which also contains thiol groups. Reducing agents containing thiol groups are known to compete with the thiol groups of cysteine residues for the formation of Co-sulfur bonds, which has been established for DTT (Getz et al., 1999).

To validate the presence of the unexpected low-spin Co(III) species, we performed EPR spectroscopy and XAS with the Co-derivative of Rxn2 and compared the results with the spectra obtained with Rxn2-CT (Figure 3). Our EPR data on Rxn2-CT and Rxn2 does not support the presence of two thiolate-ligated Co(II) ions in full-length Rxn2 (Figure 3A) and the low-spin Co(III) species proposed based on the band at 490 nm in the CD spectrum is EPR-silent. This Co(III) species is in good agreement with the +1 eV shift of the Co HERFD XAS edge energy (Figure 3B). Furthermore, the EXAFS indicate coordination by lighter atoms at shorter bond lengths (Figure S5). Taken together, the CD, EPR and XAS data support the presence of an alternative metal-binding site within the N-terminal domain of Rxn2 comprising amino acid residues 1-50. We speculate that this unspecific binding site is more exposed to the solvent compared to the active site of the rubredoxin domains and, thus, the coordinated Co(II) is readily oxidized by air oxygen. To elucidate whether this alternative binding site in the N-terminal domain is relevant *in vivo*, we isolated and characterized full-length Rxn2 from Fe-depleted and Co-supplemented minimal medium. The absorption spectrum clearly reveals a Co(II) coordinated by four thiols, supporting the incorporation of Co into the active site inside the cell (Figure 5A). The quantification of the metal content by ICP-MS support the binding of one Co per monomer (Figure 5B). The presence of one Co in the two domain Rxn2 suggests that the low-spin Co(III) species may not be relevant for the biological function of the protein.

In summary, we have reported the first biophysical investigation of the C-terminal domain of Rxn2 with Co

replacing the native metal in the active site, which is an excellent model system for artificial Co-sulfur proteins. This study presents the most in-depth spectroscopic characterization of a Co-substituted rubredoxin protein, establishing the coordination of a high-spin Co(II) to the four cysteine residues in the active site of Rxn2-CT with a pseudo-tetrahedral coordination environment. In addition, the present work shows that, under the reported conditions, only the C-terminal domain, but not the N-terminal domain, is capable of binding Co(II) in the active site. We therefore propose distinct roles for the two metal-binding domains of Rxn2. Ambivalent findings in previous studies using reconstituted Co-derivatives are most likely the result of an alternative Co-binding site in the N-terminal domain of Rxn2, which seems not to be biologically relevant.

# Materials and methods

### Chemicals and buffers

Inorganic chemicals were of analytical grade or better. For all metal binding experiments, the buffers were prepared heavy metal-free using Chelex 100 chelating resin (Biorad Laboratories, Hercules, CA, USA). The resin was treated with 2 bed volumes 1 M HCl and 2 bed volumes 1 M NaOH, followed by a washing step with 5 bed volumes Milli-Q water. Subsequently the heavy metals were removed from the buffer using the column protocol.

### Construct design and cloning

The *alkG* gene, encoding the full-length *P. putida* Rxn2 (UniProtKB accession number P00272), formerly known as *P. oleovorans*, was obtained as DNA strings by GeneArt (Thermo Fisher Scientific, Waltham, MA, USA) including an additional sequence to generate an overlap with the vector. The plasmid pET16b-TEV (gift from M. Etzkorn; Heinrich Heine University Düsseldorf, Germany) was linearized using the primers 5′-TAA CTA GCA TAA CCC CTT GGG GC-3′ and 5′-CATA TGT CCC TGA AAA TAC AGG TTT TCA TGG C-3′. The gene encoding for the C-terminal domain (amino acids 51-173) of Rxn2 was cloned using the primers 5′-GAA CAG ATT GGT GGT ATG CTG ATT GAA AGC GGT GTG-3′ and 5′-AGC AGC CGG ATC TCA TTT TTC TTC GTA CAG AAC GTA ATC TTC TTT G-3′ with pET16b-TEV-*alkG* as template. The vector pET-SUMOadapt (gift from P. Bayer; University of Duisburg-Essen, Germany) was linearized using the primers 5′-TGA GAT CCG GCT GCT AAC AAA GCC-3′ and 5′-ACC ACC AAT CTG TTC TCT GTG AGC-3′. All polymerase chain reactions were performed with the Phusion High-Fidelity DNA Polymerase (New England Biolabs, Ipswich, MA, USA). The plasmids pET16b-TEV-*alkG* and pET-SUMOadapt-*alkG*-CT were engineered using the In-Fusion HD cloning kit (Takara Bio, Kisatsu, Japan) and verified by sequencing (GATC Biotech, Konstanz, Germany).

### Protein purification

*Escherichia coli* BL21 (DE3) cells bearing the plasmid pET16b-TEV-*alkG* were cultivated in 2× Yeast Extract Tryptone (2YT) media supplemented with 100 mg/l ampicillin and OverExpress C41 (DE3) cells bearing the plasmid pET-SUMOadapt-*alkG*-CT were cultivated in Terrific Broth (TB) media supplemented with 50 mg/l kanamycin. The cells were cultured at 37°C until the optical density at 600 nm reached 0.8. Afterwards, expression was induced by addition of isopropyl-β-D-galactopyranoside to a final concentration of 0.5 mM. Cells were incubated for 16 h at 30°C, then harvested by centrifugation for 15 min at 4000*g* and 4°C, and stored at –20°C. To isolate the protein cells were thawed, resuspended in buffer A (50 mM Tris/HCl, pH 7.6, 150 mM NaCl) and 10 µg DNase I (Hoffmann-La Roche, Basel, Switzerland) were added per g cell pellet as well as a complete ULTRA protease inhibitor cocktail tablet (Hoffmann-La Roche, Basel, Switzerland). After stirring at 4°C for 1 h, the suspension was sonicated (Bandelin electronic, Berlin, Germany) for 15 min with an amplitude of 50% and a pulse of 1 s every 4 s using a VS70/T sonotrode. Cellular debris was pelleted by centrifugation for 1 h at 40 000*g* and 4°C, then applied to a Protino Ni-NTA Agarose column (Macherey-Nagel, Düren, Germany) with a bed volume of 5 ml equilibrated in buffer A using an ÄKTAprime plus system (GE Healthcare, Little Chalfont, UK). Afterwards, the column was washed with buffer A containing 12.5 mM imidazole, and the target protein was then eluted by buffer A supplemented with 250 mM imidazole. Fractions with a reddish color were pooled, desalted in buffer A and diluted to 1 mg/ml protein. After addition of 1 mM EDTA and 1 mM DTT the poly-histidine tag was cleaved by treatment of the protein with TEV protease or Ulp1 protease for 24 h at 4°C for Rxn2 or Rxn2-CT, respectively. The reaction components were removed by dialysis in buffer A before applying the protein solution on a Protino Ni-NTA column (Macherey-Nagel, Düren, Germany) to separate the uncleaved protein, the poly-histidine tag and the protease from the target protein. The obtained reddish protein solution was then precipitated in 10% TCA and pelleted by centrifugation for 15 min at 13 200*g* and 4°C. The cell pellet was washed with acetone at 4°C, followed by centrifugation three times, then dried 1 h at room temperature in an anaerobic chamber (Coy Laboratory Products, Grass Lake, MI, USA).

### Metal-binding studies

For the titration experiments with Co, TCA-precipitated protein was resolubilized in 50 mM HEPES, pH 7.5, 150 mM NaCl and reduced by 1 mM TCEP. Up to 400 µM $CoCl_2$ were added stepwise to 100 µM protein, and monitored by EAS. Reference spectra of a sample consisting of 50 mM HEPES, pH 7.5, 150 mM NaCl were used as baseline.

### Determination of the metal content

Up to 25 µM $CoCl_2$ were added to 10 µM protein after reduction with 100 µM TCEP, and incubated under gentle shaking for 16 h at 4°C. After transferring the protein into 20 mM HEPES, pH 7.5, 150 mM NaCl using a Sephadex G-25 desalting column (GE Healthcare, Little Chalfont, UK), the samples were digested in 3% trace-metal grade nitric acid before analysis. All samples were prepared in triplicates and three aliquots from each sample were analyzed. Protein concentrations were determined using tryptophan, tyrosine, and cysteine

absorbance at 280 nm. The extinction coefficients were calculated based on the amino acid sequence using the protein analysis tool ProtParam on the ExPASy server (Gasteiger et al., 2005) and are 34 200 $M^{-1}$ $cm^{-1}$ for Rxn2 and 18 500 $M^{-1}$ $cm^{-1}$ for Rxn2-CT. The Co, Fe and Zn contents of the samples were determined by inductively coupled plasma mass spectrometry using an Agilent 7500ce ICP-MS instrument (Agilent Technologies, Ratingen, Germany) in the Central Institute for Engineering, Electronics and Analytics (ZEA-3) at Forschungszentrum Jülich. The measurements were performed in collision cell mode using helium to minimize spectral interferences.

### Reconstitution of Co-rubredoxin

Samples for EAS, EPR spectroscopy and XAS were prepared using TCA-precipitated protein, which was resolubilized in 50 mM HEPES, pH 7.5, 150 mM NaCl supplemented with 0.25 mM $CoCl_2$ and 0.5 mM TCEP at 10°C for 16 h under gentle shaking. The protein was then transferred into 50 mM HEPES, pH 7.5, 150 mM NaCl by Sephadex G-25 chromatography or dialysis. The volume of the solution was adjusted to yield a final protein concentration of 1.2 mM, unless otherwise noted.

### Electronic absorption and circular dichroism spectroscopies

Electronic absorption spectra were collected on a Cary-60 spectrophotometer (Agilent Technologies, Ratingen, Germany) with 1 nm bandwidth, a scanning speed of 120 nm/min, an average time of 0.5 s in a 1 cm path length quartz cuvette at room temperature.

CD spectra were collected on a Jasco J-815 Circular dichroism spectrometer (Jasco Germany, Pfungstadt, Germany) with a scanning speed of 100 nm/min and a bandwidth of 5 nm in a 2 mm path length quartz cuvette. For the far-UV CD measurements, samples were prepared using reconstituted protein, then transferred into 10 mM sodium phosphate at pH 8.0 with a final protein concentration of 15 µM (Rxn2-CT) or 11 µM (Rxn2). An average of 20 scans was collected at 20°C with 1 nm resolution.

### EPR spectroscopy

X-band (9.64 GHz) continuous-wave EPR spectra were collected on a Bruker ESP300E spectrometer (Oxford Instruments, Abingdon-on-Thames, UK) equipped with a helium flow cryostat ESR910 and an ITC 503 temperature controller. The EPR spectrum was simulated with the EasySpin (v 5.2.2) (Stoll and Schweiger, 2006) for Matlab.

### X-ray spectroscopy

High energy resolution X-ray absorption spectra were collected at beam line ID26 (6 GeV, 200 mA) of the European Synchrotron Radiation Facility (ESRF) in Grenoble, France. The incident beam was monochromatized with a liquid nitrogen cooled Si(311) monochromator and focused to a spot size of 100 (w) × 15 (v) micron spot size on the sample. The incident energy was calibrated by adjusting the first inflection point of a Co foil XAS spectrum to 7713.6 eV. The Co XAS spectra were collected by monitoring the fluorescence of the maximum of the Co Kα emission feature (6.9313 keV) employing a Johann spectrometer with five Si(531) analyzer crystals at a 1 M radii Rowland geometry. A silicon-drift Ketek detector windowed to the Co Kα emission was utilized to further reduce background noise. All spectra were collected at 20 K in a liquid helium cryostat to reduce radiation damage. Sequential fast XAS scans in conjunction with movement of the sample were collected and evaluated at the beam line within PyMCA (Solé et al., 2007) for signs of radiation damage to determine maximum dwell time per sample spot.

The raw XAS spectra were initially averaged in Matlab and exported for further processing within Athena (Ravel and Newville, 2005). A second order polynomial was fit to the pre-edge region and subtracted throughout the entire EXAFS spectrum. A three-region cubic spline (with the AUTOBK function within Athena) was employed to model the background function to a minimum of $k = 14$ $Å^{-1}$ for all spectra. Fourier-transforms were performed over a $k$ range of 2–11.5 $Å^{-1}$ and are presented without a phase shift correction.

EXAFS scattering paths were calculated with FEFF6 using Demeter v0.9.24 (Ravel and Newville, 2005). The scattering paths were calculated from a Rubredoxin homolog, PDB accession code 1R0H. Only atoms within 8 Å of the metal site were used as coordinates for the FEFF input. The following FEFF flags were used: RMAX 4; and NLEGS 3. The Fourier transform of the $k^3$-weighted EXAFS was fit over the $R$ space of 1–3 Å. By grouping similar scattering paths of a common coordination shell and increasing its degeneracy, n, the number of variables used for that coordination shell is minimal, two variables: $\sigma^2$ and $\Delta R$. A single $\Delta E_0$ variable is used for all paths of a single model. The total amplitude of the EXAFS fit was set to 0.9.

## Additional information

Supplementary Figures S1–S5, Table S1, and supplementary methods are available online.

**Acknowledgments:** This work was supported by the Fonds der Chemischen Industrie, Liebig Fellowship to I.S. and a PhD fellowship to L.M.G. The authors also thank the Alexander von Humboldt Foundation (to G.E.C) and the Max-Planck-Gesellschaft (to S.D.). The European Synchrotron Radiation Facility is acknowledged for providing beamtime and for technical support from Lucia Amidani at beam line ID26. We gratefully acknowledge the performance of ICP-MS measurements by Ulrike Seeling and Astrid Küppers, ESI-MS measurements by Sabine Metzger at Leibniz Research Institute for Environmental Medicine, purification using HPLC by Nadine Rösener and Lothar Gremer, and IR spectroscopic measurements by Claudia Hoppen and Georg Groth. We are also grateful to Manuel Etzkorn and Peter Bayer for providing plasmids, and Dieter Willbold for the laboratory facilities. We acknowledge networking support to L.M.G. and I.S. from the COST action FeSBioNet (contract CA15133).

**Conflict of interest statement:** The authors declare that they have no conflict of interest regarding the contents of this article.

## References


Anglin, J.R. and Davison, A. (1975). Iron(II) and cobalt(II) complexes of Boc-(Gly-L-Cys-Gly)4-NH2 as analogs for the active site of the iron-sulfur protein rubredoxin. Inorg. Chem. *14*, 234–237.

Bencini, A., Bertini, I., Canti, G., Gatteschi, D., and Luchinat, C. (1981). The epr spectra of the inhibitor derivatives of cobalt carbonic anhydrase. J. Inorg. Biochem. *14*, 81–93.

Bordeaux, M., Galarneau, A., and Drone, J. (2012). Catalytic, mild, and selective oxyfunctionalization of linear alkanes: current challenges. Angew. Chem. Int. Ed. *51*, 10712–10723.

Bradford, M.M. (1976). A rapid and sensitive method for the quantitation of microgram quantities of protein utilizing the principle of protein-dye binding. Anal. Biochem. *72*, 248–254.

Castillo, R.G., Banerjee, R., Allpress, C.J., Rohde, G.T., Bill, E., Que, L., Lipscomb, J.D., and DeBeer, S. (2017). High-energy-resolution fluorescence-detected X-ray absorption of the Q intermediate of soluble methane monooxygenase. J. Am. Chem. Soc. *139*, 18024–18033.

Curdel, A. and Iwatsubo, M. (1968). Biosynthetic incorporation of cobalt into yeast alcohol dehydrogenase. FEBS Lett. *1*, 133–136.

Dauter, Z., Wilson, K.S., Siekert, L.C., Moulist, J.-M., and Meyer, J. (1996). Zinc-and iron-rubredoxins from *Clostridium pasteurianum* at atomic resolution: a high-precision model of a ZnS4 coordination unit in a protein. Biochemistry *93*, 8836–8840.

Drum, D.E. and Vallee, B.L. (1970). Optical properties of catalytically active cobalt and cadmium liver alcohol dehydrogenases. Biochem. Biophys. Res. Commun. *41*, 33–39.

Edelhoch, H. (1967). Spectroscopic determination of tryptophan and tyrosine in proteins. Biochemistry *6*, 1948–1954.

Fukui, K., Ohya-Nishiguchi, H., and Hirota, N. (1991). ESR and magnetic susceptibility studies on high-spin tetrahedral cobalt(II)–thiolate complexes: an approach to rubredoxin-type active sites. Bull. Chem. Soc. Jpn. *64*, 1205–1212.

Gasteiger, E., Hoogland, C., Gattiker, A., Duvaud, S., Wilkins, M.R., Appel, R.D., and Bairoch, A. (2005). Protein identification and analysis tools on the ExPASy server. In: The Proteomics Protocols Handbook, John M. Walker, ed. (Totowa, NJ, USA: Humana Press), pp. 571–607.

Gavel, O.Y., Bursakov, S.A., Calvete, J.J., George, G.N., Moura, J.J.G., and Moura, I. (1998). ATP sulfurylases from sulfate-reducing bacteria of the genus *Desulfovibrio*. A novel metalloprotein containing cobalt and zinc. Biochemistry *37*, 16225–16232.

Getz, E.B., Xiao, M., Chakrabarty, T., Cooke, R., and Selvin, P.R.A. (1999). A comparison between the sulfhydryl reductants tris(2-carboxyethyl)phosphine and dithiothreitol for use in protein biochemistry. Anal. Biochem. *273*, 73–80.

Gill, S.C. and von Hippel, P.H. (1989). Calculation of protein extinction coefficients from amino acid sequence data. Anal. Biochem. *182*, 319–326.

Good, M. and Vasak, M. (1986). Spectroscopic properties of the cobalt(II)-substituted α-fragment of rabbit liver metallothionein. Biochemistry *25*, 3328–3334.

Kok, M., Oldenhuis, M., van der Linden, M.P.G., Meulenberg, C.H.C., Kingma, J., and Withold, B. (1989). The *Pseudomonas oleovorans* alkBAC operon encodes two structurally related rubredoxins and an aldehyde dehydrogenase. J. Biol. Chem. *264*, 5442–5451.

Lee, H.J., Lian, L.Y., and Scrutton, N.S. (1997). Recombinant two-iron rubredoxin of *Pseudomonas oleovorans*: overexpression, purification and characterization by optical, CD and $^{113}$Cd NMR spectroscopies. Biochem. J. *328*, 131–136.

Lode, E.T. and Coon, M.J. (1971). Enzymatic omega-oxidation. V. Forms of *Pseudomonas oleovorans* A containing one or two iron atoms: structure and function in omega-hydroxylation. J. Biol. Chem. *246*, 791–802.

Lovenberg, W. and Sobel, B.E. (1965). Rubredoxin: a new electron transfer protein from *Clostridium pasteurianum*. Proc. Natl. Acad. Sci. USA *54*, 193–199.

Maher, M., Cross, M., Wilce, M.C.J., Guss, J.M., and Wedd, A.G. (2004). Metal-substituted derivatives of the rubredoxin from *Clostridium pasteurianum*. Acta Crystallogr. D Biol. Crystallogr. *60*, 298–303.

Majtan, T., Freeman, K.M., Smith, A.T., Burstyn, J.N., and Kraus, J.P. (2011). Purification and characterization of cystathionine β-synthase bearing a cobalt protoporphyrin. Arch. Biochem. Biophys. *508*, 25–30.

Makinen, M.W., Kuo, L.C., Yim, M.B., Wells, G.B., Fukuyama, J.M., and Kim, J.E. (1985). Ground term splitting of high-spin cobalt(2+) ion as a probe of coordination structure. 1. Dependence of the splitting on coordination geometry. J. Am. Chem. Soc. *107*, 5245–5255.

Maret, W. and Vallee, B.L. (1993). Cobalt as probe and label of proteins. Methods Enzymol. *226*, 52–71.

May, S.W. and Kuo, J.Y. (1978). Preparation and properties of cobalt(II) rubredoxin. Biochemistry *17*, 3333–3338.

McMillin, D.R., Holwerda, R.A., and Gray, H.B. (1974). Preparation and spectroscopic studies of cobalt(II)-stellacyanin. Proc. Natl. Acad. Sci. USA *71*, 1339–1341.

Moura, I., Teixeira, M., Moura, J.J.G., and LeGall, J. (1991). Spectroscopic studies of cobalt and nickel substituted rubredoxin and desulforedoxin. J. Inorg. Biochem. *44*, 127–139.

Perry, A., Lian, L.Y., and Scrutton, N.S. (2001). Two-iron rubredoxin of *Pseudomonas oleovorans*: production, stability and characterization of the individual iron-binding domains by optical, CD and NMR spectroscopies. Biochem. J. *354*, 89–98.

Perry, A., Tambyrajah, W., Grossmann, J.G., Lian, L.Y., and Scrutton, N.S. (2004). Solution structure of the two-iron rubredoxin of *Pseudomonas oleovorans* determined by NMR spectroscopy and solution X-ray scattering and interactions with rubredoxin reductase. Biochemistry *43*, 3167–3182.

Ravel, B. and Newville, M. (2005). ATHENA, ARTEMIS, HEPHAESTUS: data analysis for X-ray absorption spectroscopy using IFEFFIT. J. Synchrotron Radiat. *12*, 537–541.

Shimizu, T., Mims, W.B., Davis, J.L., and Peisach, J. (1983). Studies of the coordination of rare earth and transition metal nucleotide complexes by an electron spin echo method. Biochim. Biophys. Acta *757*, 29–39.

Stoll, S. and Schweiger, A. (2006). EasySpin, a comprehensive software package for spectral simulation and analysis in EPR. J. Magn. Reson. *178*, 42–55.

Strug, I., Utzat, C., Cappione, A., Gutierrez, S., Amara, R., Lento, J., Capito, F., Skudas, R., Chernokalskaya, E., and Nadler, T. (2014). Development of a univariate membrane-based mid-infrared

method for protein quantitation and total lipid content analysis of biological samples. J. Anal. Methods Chem. *2014*, 1–12.

Sugiura, Y. (1978). Electronic properties of sulfhydryl- and imidazole-containing peptide-cobalt(II) complexes: their relationship to cobalt(II)-substituted "blue" copper proteins. Bioinorg. Chem. *8*, 453–460.

Thomas, J.M., Raja, R., Sankar, G., and Bell, R.G. (2001). Molecular sieve catalysts for the regioselective and shape-selective oxyfunctionalization of alkanes in air. Acc. Chem. Res. *34*, 191–200.

Tsai, Y.-F., Luo, W.-I., Chang, J.-L., Chang, C.-W., Chuang, H.-C., Ramu, R., Wei, G.-T., Zen, J.-M., and Yu, S.S.-F. (2017). Electrochemical hydroxylation of C3–C12 n-alkanes by recombinant alkane hydroxylase (AlkB) and rubredoxin-2 (AlkG) from *Pseudomonas putida* GPo1. Sci. Rep. *7*, 1–13.

van Beilen, J.B., Neuenschwander, M., Smits, T.H.M., Roth, C., Balada, S.B., and Witholt B. (2002). Rubredoxins involved in alkane oxidation. J. Bacteriol. *184*, 1722–1732.

Westre, T.E., Kennepohl, P., DeWitt, J.G., Hedman, B., Hodgson, K.O., and Solomon, E.I. (1997). A multiplet analysis of Fe K-edge 1s → 3d pre-edge features of iron complexes. J. Am. Chem. Soc. *119*, 6297–6314.

Zielazinski, E.L., Cutsail, G.E., Hoffman, B.M., Stemmler, T.L., and Rosenzweig, A. (2012). Characterization of a cobalt-specific $P_{1B}$-ATPase. Biochemistry *51*, 7891–7900.

**Supplemental Material:** The online version of this article offers supplementary material (https://doi.org/10.1515/hsz-2018-0142).